Available online at www.sciencedirect.com
ScienceDirect
Trans. Nonferrous Met. Soc. China 23(2013) 3525−3539

Transactions of Nonferrous Metals Society of China
www.tnmsc.cn

Influence of FSW parameters on formation quality and mechanical properties of Al 2024-T351 butt welded joints

I. RADISAVLJEVIC[1], A. ZIVKOVIC[2], N. RADOVIC[3], V. GRABULOV[4]

1. Military Technical Institute, Belgrade, Serbia;
2. GOSA FOM, Smederevska Palanka, Serbia;
3. Faculty of Technology and Metallurgy, University of Belgrade, Belgrade, Serbia;
4. Institute for Materials testing, Belgrade, Serbia

Received 19 April 2013; accepted 16 September 2013

Abstract: The influence of *R*/*v* ratio on joint quality in 2024-T351 aluminum alloy was studied. Specimens were subjected to friction stir welding with the rotation rates of 750, 950 and 1180 r/min and welding speed between 73 and 190 mm/min, providing *R*/*v* ratio between 5.00 and 10.27. The welded joints were tested by means of both non-destructive (visual, penetrant and X-ray inspection) and destructive (metallographic, tension and hardness) testing. In all specimens typical zones are revealed, with corresponding differences in grain size. Tensile efficiency of the joints obtained is in the range of 52.2% to 82.3%. The results show that the best quality is obtained at *R*/*v* ratio of 8.06, 10.17 and 10.27. This behavior is attributed to the assumption that the material flows around the pin with an optimal speed, i.e. sufficient amount of material is available to fill the gap and prevent tunnel formation. *R*/*v* ratio also showed influence on hardness distribution, onion features and crack initiation/propagation zones.
Key words: Al 2024 alloy; friction stir welding; welding parameters; heat input; weld quality

1 Introduction

Heat treatable 2xxx series aluminum alloys with high strength level, favorable strength to mass ratio and good damage tolerance, are widely used for structural applications. Extensive use of the age hardenable 2xxx series aluminum alloys was hampered by limitations imposed by joining techniques. The loss of strength in the components fabricated from these alloys, using conventional, high heat input, fusion welding techniques such as TIG or MIG, introduced a serious limitation in their exploitation due to the presence of porosity, slag inclusion, solidification cracks, distortion, etc. Gap between the strength values of the fusion joint and the parent material is more than 40%, resulting in the fact that mechanical joints are preferred. In order to solve this difficulty a solid state joining process, named friction stir welding (FSW), was invented. At present, FSW is increasingly applied to the aerospace, automotive, marine and military industries [1−9].

FSW offers several advantages over conventional fusion welding process because of its low heat input and absence of melting and solidification process, enabling welding of materials that are extremely difficult to weld by conventional fusion welding processes, such as 2xxx and 7xxx series aluminum alloys. The benefits therefore include low distortion and residual stresses, no loss of alloying elements, no arc, no fume and no filler wire. Thus FSW becomes a very suitable process for joining high strength aluminum alloy such as 2024 [10−15].

Compared with the conventional fusion welding, different zones are formed during FSW due to friction heat and plastic deformation. Frictional heat causes metal softening and thus allows the tool move along the joint line. Under the driving of the welding tool (shoulder and pin), structure of weld, due to severe mechanical stresses experienced by material, shows three distinct microstructural zones on the transverse cross section of the FSW joint, i.e., nugget zone (NZ), thermo-mechanically affected zone (TMAZ) and heat affected zone (HAZ). The NZ is a region through which tool pin passes and thus experiences both high deformation and heat treatment. It generally consists of very fine equiaxed

Corresponding author: I. RADISAVLJEVIC; Tel: +381-11-2051278; Fax: +381-11-2508474; E-mail: igra@sbb.rs; vti@vti.vs.rs
DOI: 10.1016/S1003-6326(13)62897-6

grains, due to full recrystallization, and characterized by the presence of so-called onion rings. Adjacent to the nugget zone is a TMAZ. This region experienced a severe thermo-mechanical alteration, though it has been not directly subjected to pin or shoulder action due to internal shear stresses. In TMAZ metal is plastically deformed as well as heated, but this is not sufficient to cause recrystallization. Beyond TMAZ there is part of material that experiences only a heating effect, with no mechanical deformation. This zone is referred as HAZ. The thin zone subjected directly to the action of tool shoulder is referred as flow arm [16−21]. Semicircular rings on the top of weld surface are referred as banded microstructure. Distance between semicircular rings depends on tool advance per revolution. Spacing between bands will increase as this ratio (welding speed/ rotation speed) grows, resulting in a less homogenous structure within the weld [22−25]. Several parameters, such as rotation rate (R), welding speed (v), axial force, tool and pin geometry, tool tilt angle and its penetration into the blanks (plunge depth) affect FSW process. Among these parameters, rotation rate and welding speed strongly influence the thermal cycle and are the two most important welding parameters [26−46].

The aim of this work is to establish the influence of R/v ratio on joint quality and elucidate defects formation mechanisms in 2024-T351 aluminum alloy.

2 Experimental

The rolled plates of 8.0 mm thickness, made of commercial aluminum alloy Alclad 2024-T351, were used in this work as the base metal. The plates were machined on both sides to remove the Alclads and get the final thickness of 6.0 mm. The chemical composition and mechanical properties of the machined plate are listed in Tables 1 and 2. The dimensions of single welded plates were 260 mm×65 mm×6 mm. The sides of plates were machined and had stiff contact with supporting plate, and were butt-welded along the rolling direction using adopted conventional milling machine. The welding length was around 210 mm on each pair of plates. The used FSW tool was made of 56 NiCrMoV7 tool steel, with spiral thread on the 5.5 mm length and concave profiled head on the 25 mm diameter cylindrical shoulder. The tool details are listed in Table 3. The tool was heat treated to HRC51. The tool tilt angle was 1.0° and was kept constant. An equal axial (welding) force was obtained by controlling the plunge depth of welding tool, since all the specimens had the same thickness. The plunge depth of tool shoulder was 0.2 mm. All welded joints were in “hot” condition, according to R/v ratio criterion suggested by VILAÇA at al [5,47]. The welding parameters used in this study are summarized in Table 4, where ratio R^2/v represents the pseudo heat index suggested by ARBEGAST and HARTLEY [48].

Table 1 Chemical composition of base metal (mass fraction, %)

Cu	Mg	Mn	Fe	Zn
4.70	1.56	0.65	0.17	0.11
Si	Ti	Zr	Ni	Cr
0.046	0.032	0.011	0.006	0.004

Table 2 Mechanical properties of base metal

YS/MPa	UTS/MPa	A_5/%	Hardness (HV)
370	481	18	145

Table 3 Geometry of used FSW tool

Pin description	Pin diameter/mm		Pin angle/(°)	Thread slope/(°)	Pitch of pin/mm
	Root	Head			
Taper screw thread pin	10	4	20	5	1.5

Table 4 Welding parameters

Sample	Rotation rate, R/(r·min^{-1})	Welding speed, v/(mm·min^{-1})	R/v	R^2/v
A	750	73	10.27	7700
B		93	8.06	6050
C		116	6.46	4850
D		150	5.00	3750
E	950	93	10.21	9700
F		190	5.00	4750
G	1180	116	10.17	12000
H		150	7.87	9280

In order to reveal the presence of surface and/or volume defects, the welded joints were first subjected to visual, penetrant, X-ray and ultrasonic examination. Further examination was performed only on the welded joints that had no defects. Complete testing procedure is given in Table 5. All the welded samples were naturally aged at room temperature for more than 20 d and the specimens were cross-sectioned perpendicular to the welding direction (Fig. 1).

Metallographic observation was carried out by optical microscopy (OM). The specimens for OM were ground, polished and etched using Tucker’s and Barker’s reagent for macro and microstructure, respectively. Electro polishing and etching technique was used on the specimen for microstructure examination. Much care was

Table 5 Testing procedure of welded joints

Type	Step	Method
Nondestructive testing	1	Visual examination
	2	Penetrant examination
	3	X-ray examination
	4	Ultrasonic examination
Destructive testing	5	Evaluation of macrostructure
	6	Evaluation of microstructure
	7	Tension testing
	8	Hardness testing
	9	SEM

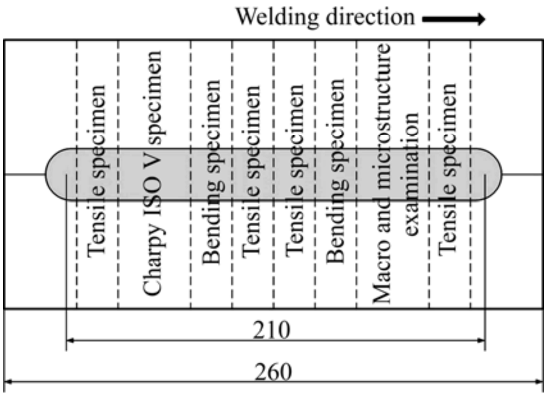

Fig. 1 Schematic of specimen location in weld (Unit: mm)

taken to ensure location-to-location correspondence between the observations and hardness measurements.

In order to obtain fracture locations of the FSW joints, the surfaces of tensile specimens were swab etched using Tucker's solution before testing. Room-temperature tensile tests were carried out according to ASTM E8M−11 at a strain rate of 3.3×10^{-3} s^{-1}. In order to assess the reproducibility, at least three tests were performed for each set of conditions.

Vickers hardness measurement was conducted perpendicular to the welding direction, using digitally controlled hardness test machine (HVS−1000) applying 9.807 N force for 15 s. The hardness profiles were obtained along 3 horizontal and 17 vertical directions (Fig. 2). In order to obtain the hardness distribution maps

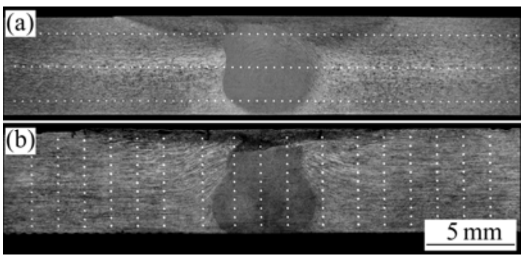

Fig. 2 Horizontal (a) and vertical (b) hardness test lines

a total of 183 and 187 indentations in horizontal and vertical directions, respectively, were measured.

3 Results

3.1 Joint quality

Figure 3 shows the upper surface macrographs of the joints under various welding parameters. At rotation rate of 750 r/min, joint surfaces of all the samples are smooth (Figs. 3(a)−(d)). At rotation rate of 950 and 1180 r/min, appearance of extensive and slight joint surface delaminating morphologies was observed (Figs. 3(e)−(h)). For both the rotation rates, the joint surfaces were rougher at lower welding speed. Also, tunnel defect was visually observed at samples F and H (Figs. 3(f) and 3(h)); further testing of these samples was not carried out.

Figure 4 shows the macrostructures of transverse cross sections of the joints welded under various welding parameters. For tunnel free joints, no other welding defects were detected. Tunnel defects at sample H were not extending throughout the whole weld length. According to the role of shoulder and pin in NZ formation, the NZ can be subdivided into three sub-zones: the shoulder-driven zone (SDZ), the pin-driven zone (PDZ), and the swirl zone (SWZ). SDZ and SWZ are more or less pronounced, due to different welding parameters. It can be seen that a comparatively large PDZ, with regular onion ring structures, a narrow SDZ and SWZ were observed. Note that the onion ring shape was not identical for all the samples and it depended on the welding parameters. Furthermore, decreasing the welding speed for same rotation rate produced finer spacing between rings. Typical onion ring structure is shown in Fig. 5.

3.2 Structure

Set of figures related to microstructure examination of welds are given in Figs. 6 and 7. Figure 6 shows the optical micrographs of the NZ and TMAZ. As a result of previous rolling process, elongated grains were observed in BM. Grain size in the NZ and part of TMAZ near to nugget is very fine (Figs. 6(a) and (c)). The NZ microstructure is characterized by recrystallized, fine equiaxed grains (Figs. 6(b) and (d)). Highly deformed structure, consisting of upward elongated grains, was observed in the TMAZ (Figs. 6(a) and (c)). On the other hand, grain structure in the HAZ is similar to the BM structure.

Due to material flow in the stirred zone, primary Al_2Cu particles were fractured during welding. It can be seen that particles fracture process is more intensive in

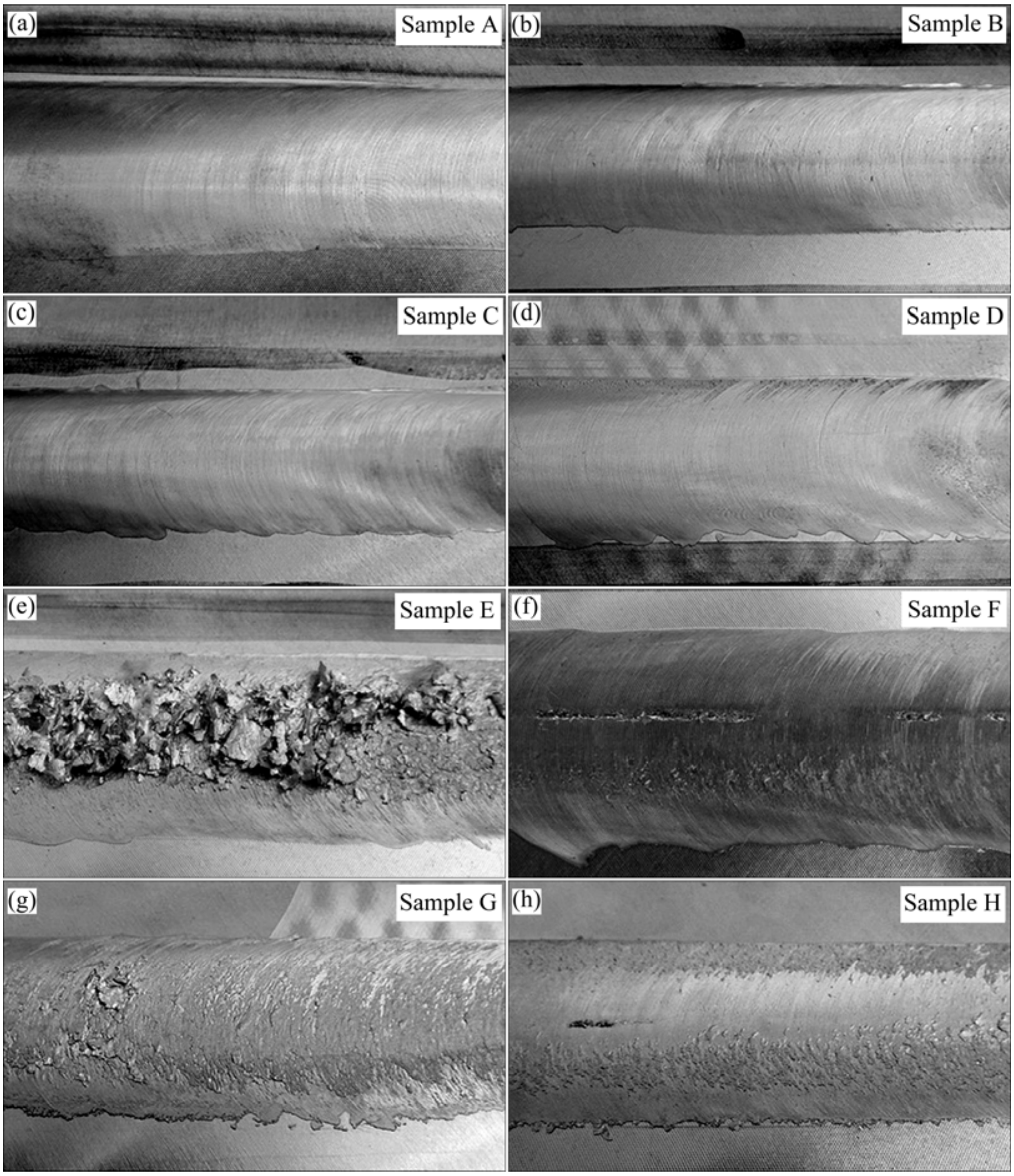

Fig. 3 Joint upper surface morphologies of specimens

the NZ than in the TMAZ. Note that particles in NZ are the finest (Fig. 7). According to this, it can be assumed that with higher rotation rate particles have been more effectively broken.

It seems that the variation of welding parameters in this work did not produce significant and clear differences in microstructure for each particular zone in different welded joints. On the other hand, overall influence of both grain refinement and fracture of Al_2Cu particles was possible to estimate by hardness measurement (see next section).

3.3 Hardness distribution

Single hardness profile could not predict joints fracture path because of the limited lowest hardness points. Thus, in order to obtain detailed hardness distribution, the hardness profiles were obtained along 3 horizontal and 17 vertical directions at a total of 183 and 187 indentations, respectively. Figures 8−11 show the joints hardness profiles under the investigated welding parameters. The welds exhibited typical W-shaped hardness profiles, characteristic for precipitation hardening aluminum alloys friction stir welds. NZ was significantly harder than the TMAZ and can reach BM hardness level. The hardness of NZ showed strong dependence on rotation rate. Two low hardness regions (LHR) were observed, one on the AS and the other on the RS. The hardness level of LHR on the AS and RS was almost equal in most cases, with some exception (Figs. 8 and 9). Detailed hardness observation at lower half and mid-thickness of the weld showed that increasing the rotation rate at constant welding speed

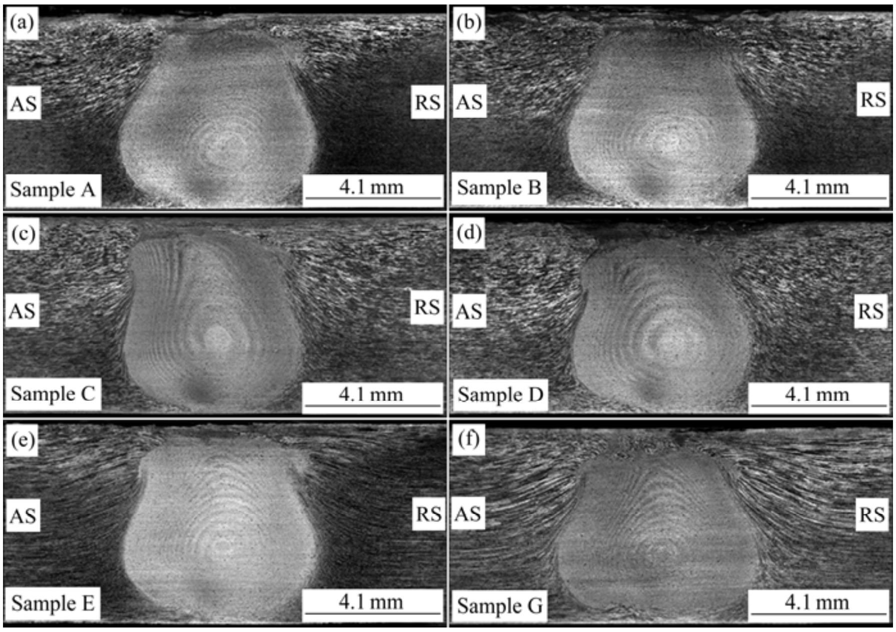

Fig. 4 Cross sectional macrostructures of joints welded under various welding parameters

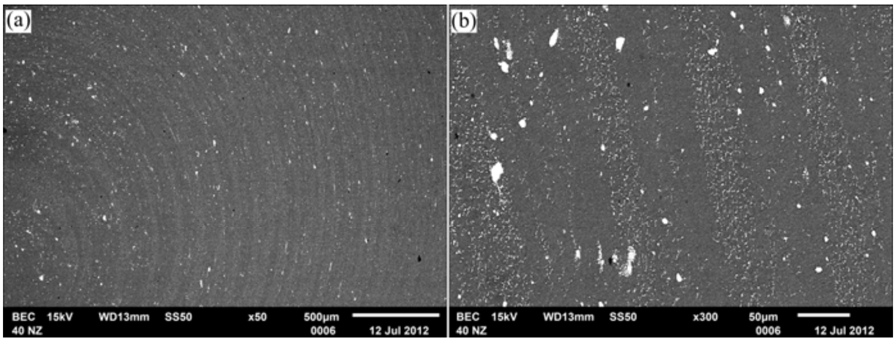

Fig. 5 SEM backscattered images of onion rings in NZ

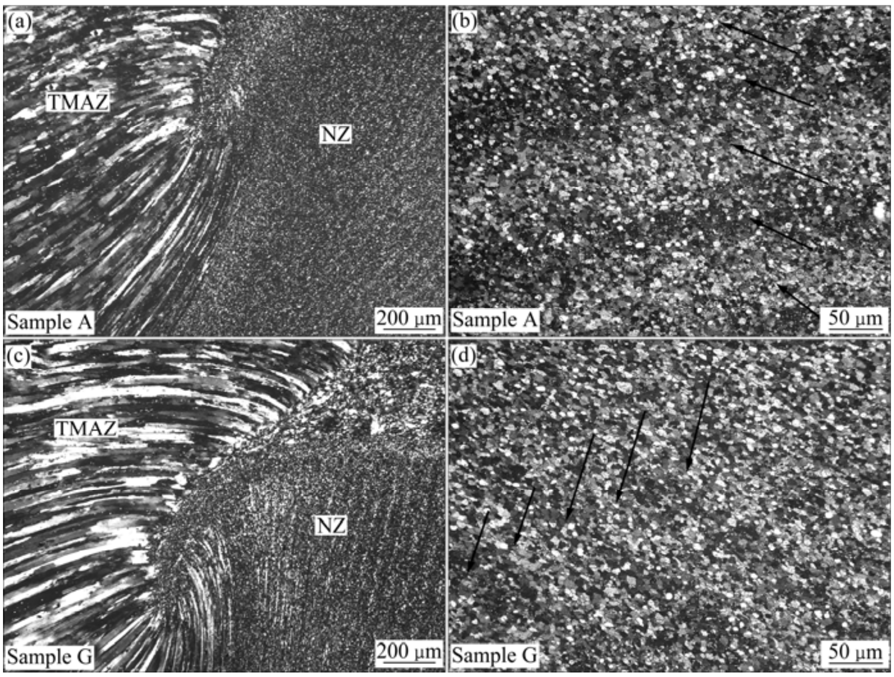

Fig. 6 Typical microstructures of joint: (a, c) contact line NZ-TMAZ on AS; (b, d) NZ

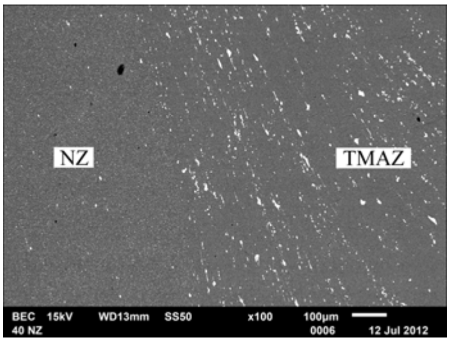

Fig. 7 SEM backscattered image of contact line between NZ and TMAZ on RS

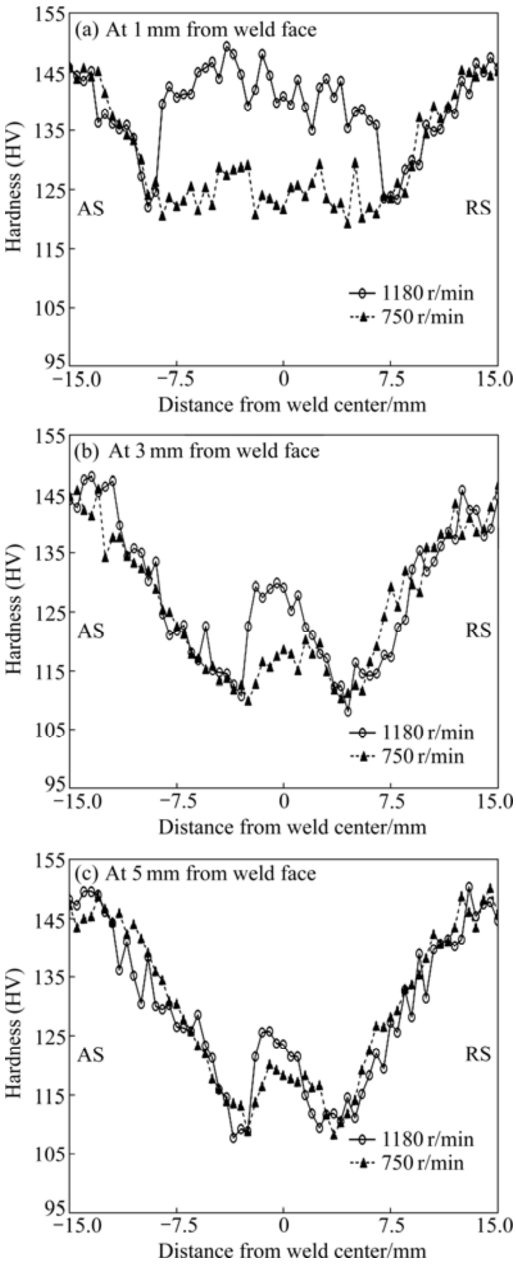

Fig. 8 Hardness distribution at cross-section of FSW 2024-T351 joints showing effect of rotation rate on hardness on different positions across weld at welding speed of 116 mm/min

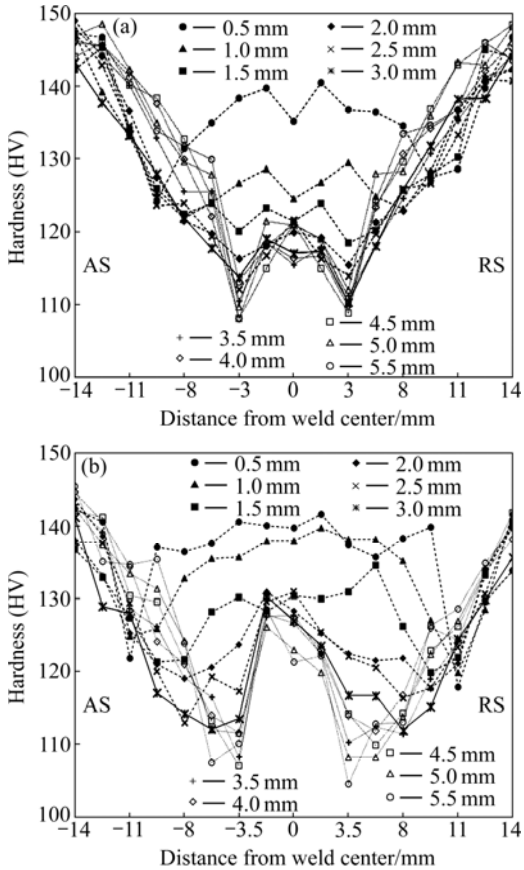

Fig. 9 Hardness profiles of welded joints with different distances from weld surface: (a) Sample C; (b) Sample G

exerted no noticeable influence on the LHR hardness level (around HV110) and showed small or medium influence on LHR position (Figs. 9(a) and 9(b), respectively). At upper half of the weld, LHR hardness level was generally higher for approximately HV10. Furthermore, the position of LHR was obviously different (greater distance from weld center) in comparison with lower half of the weld (Figs. 8(a) and 9). On the other hand, increasing the welding speed at constant rotation rate generally increased NZ and LHR hardness, but did not have noticeable influence on LHR position (Fig. 10). LHR hardness was greater at upper part of the weld. In detailed hardness observation at constant rotation rate of 750 r/min, one phenomenon was observed for the welding speed of 73 mm/min. Namely, LHR hardness at mid-thickness of the weld in comparison with lower part of weld on RS was essentially unchanged, contrary at AS (Figs. 10(b) and (c)). At upper part of weld, LHR hardness on RS rose and was approximately equal to LHR hardness on AS (Fig. 10(a)). Also, at these parts of weld, for 73 mm/min welding speed, LHR position and hardness on RS were dramatically different in comparison with those under other welding speeds (Figs. 10(a) and 10(b)). Note that

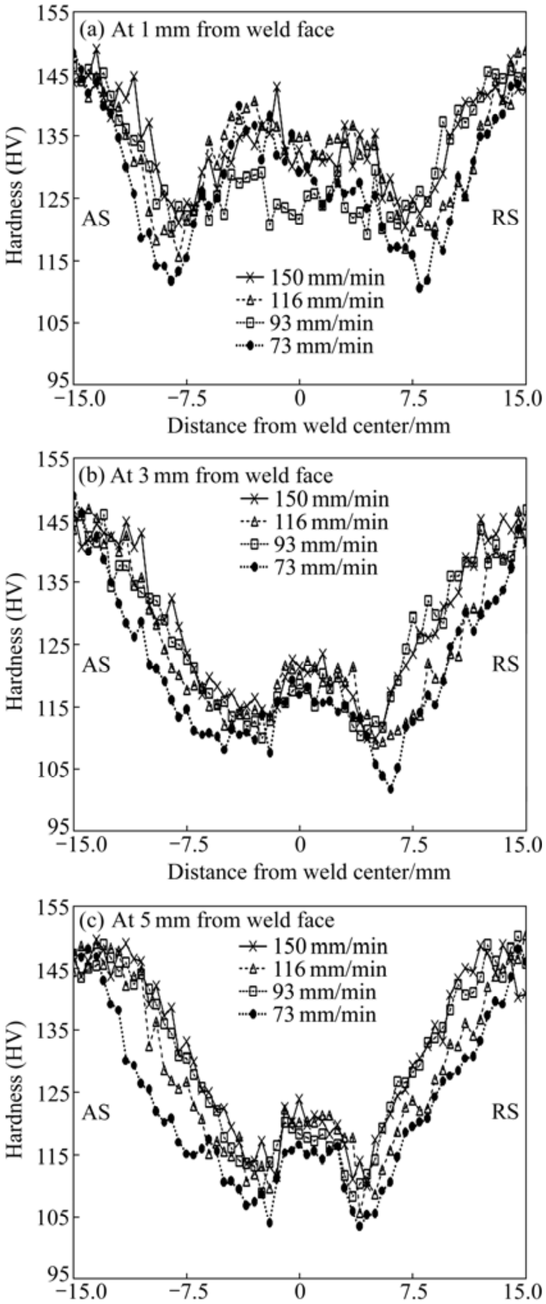

Fig. 10 Hardness distribution at cross-section of FSW 2024-T351 joints showing effect of different welding speed on hardness profiles on different positions across weld at rotate rate of 750 r/min

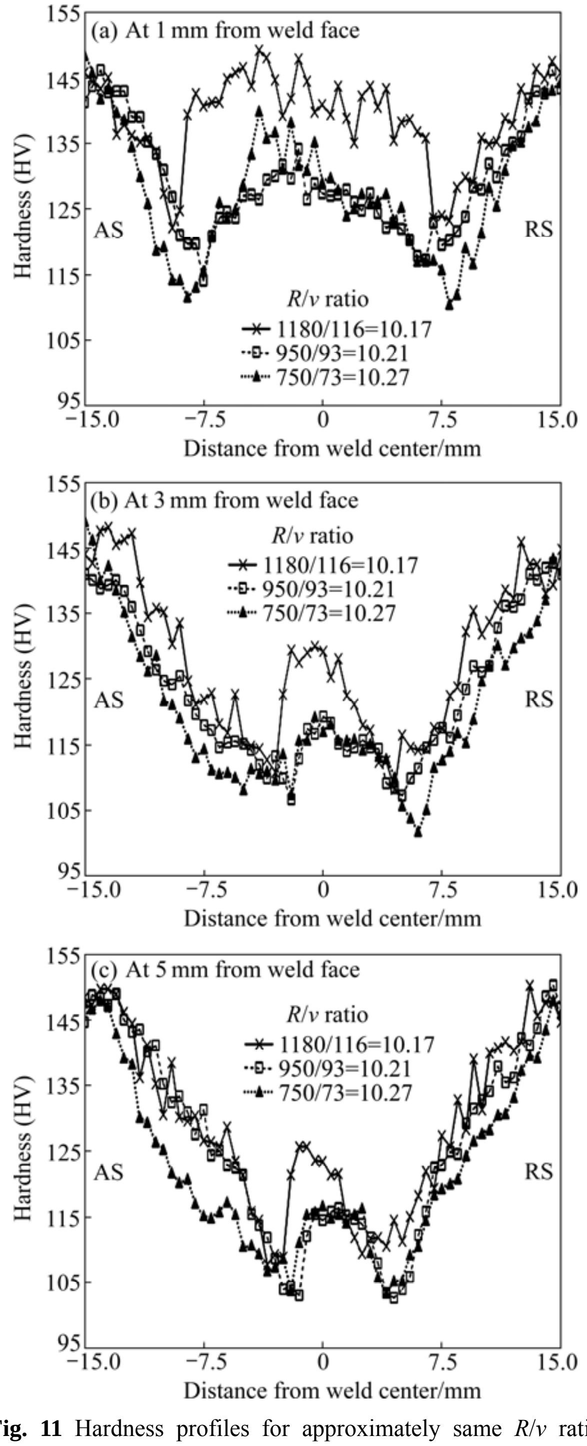

Fig. 11 Hardness profiles for approximately same R/v ratio (R/v≈10)

NZ hardness, for 116 mm/min welding speed at upper and middle part of the weld, was on the same level. Furthermore, hardness at upper weld part for this welding speed was the lowest (Fig. 10(a)). However, hardness distributions across the FSW joints were essentially non-homogenous and showed strong dependence on the welding parameters. For previously discussed observations, it is interesting to compare the hardness profiles for samples with approximately same R/v ratio (Fig. 11).

In order to accurately predict the joints fracture behavior, according to the opinion that the fracture location is a direct reflection of the weakest part of joint, the detailed hardness contour maps are plotted (Fig. 12). It can be determined that the LHZ was generally located at the TMAZ, rather on part of TMAZ near to contact line between NZ and TMAZ (Fig. 7).

3.4 Tensile properties and fracture behavior

The tensile properties and fracture location of joint

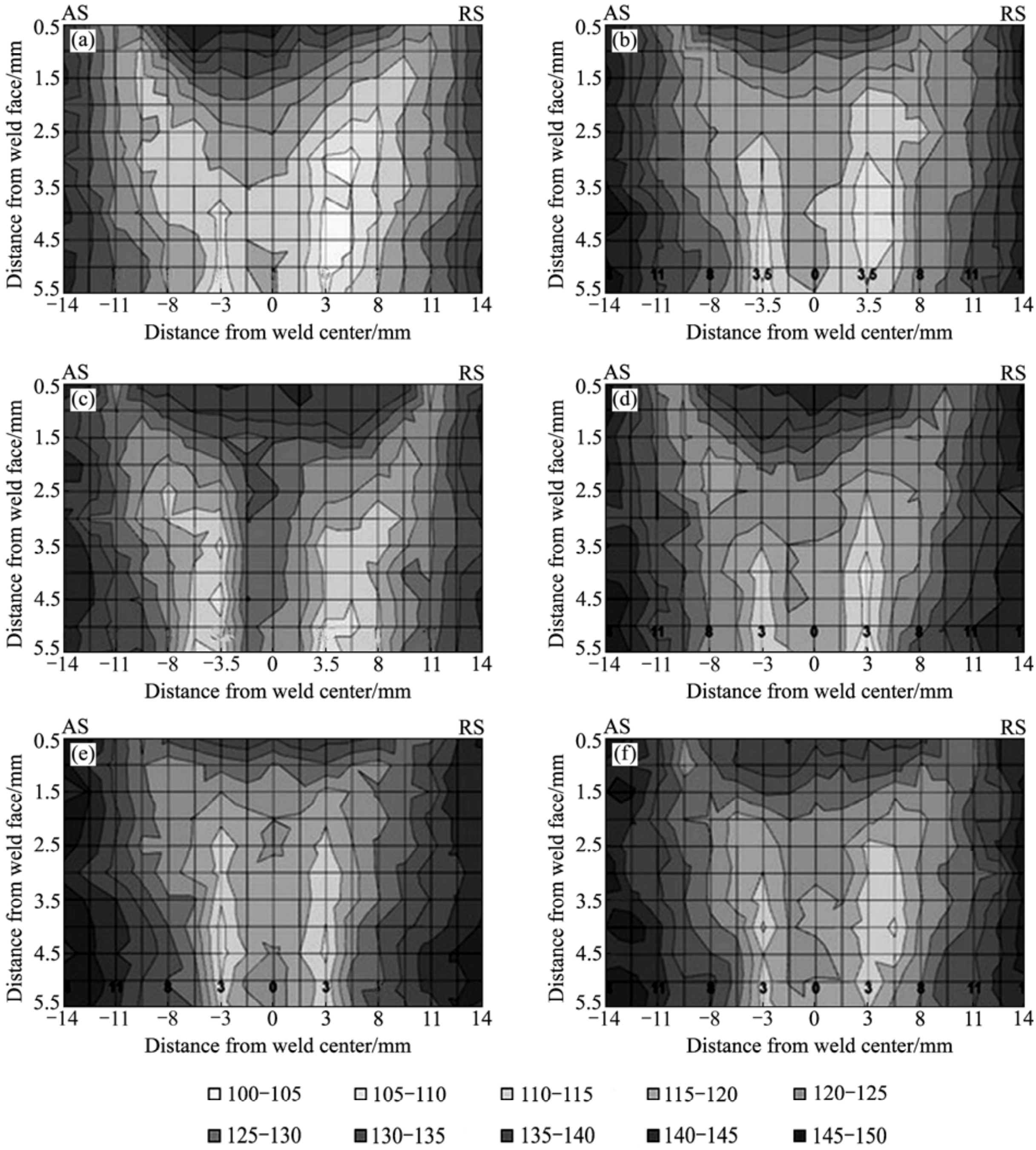

Fig. 12 Detailed hardness contour maps of welded joints: (a) Sample A, R/v=10.27; (b) Sample E, R/v=10.21; (c) Sample G, R/v=10.17; (d) Sample B, R/v=8.06; (e) Sample C, R/v=6.46; (f) Sample D, R/v=5.00

under investigated welding parameters are shown in Table 6 and Fig. 13. It is found that: 1) under constant rotation rate of 750 r/min, the tensile strength generally decreased when the welding speed was increased (Fig. 13); sharp decrease of UTS and elongation was observed when the welding speed increased from 73 to 116 mm/min. At welding speed of 150 mm/min slight increase of tensile strength was present; 2) under constant welding speed of 93 and 116 mm/min, increasing rotation rate from 750 to 950 r/min (samples B and E) or from 750 to 1180 r/min (samples C and G) had opposite effect. Namely, in the first case slight drop of tensile properties was observed while in the second case tensile properties showed significant amplification (Fig. 14(b)). The obtained UTS values for weld joint and base metal showed that UTS_{FSW}/UTS_{BM} ratio was up to 83%. Crack initiation in most cases was in the thermo-mechanically affected zone on the AS, very close to the nugget. The tensile properties of each joint were lower than those of base material and the elongation of

Table 6 Transverse tensile properties and fracture location of FSW 2024-T351 joints

Sample	UTS/MPa	A_5/%	Joint efficiency		Fracture location	R/v
			(UTS_{FSW}/UTS_{BM})/%	(A_{FSW}/A_{BM})/%		
A	403	8.0	83.4	44.4	TMAZ/HAZ interface on RS	10.27
	379	6.6	78.8	36.7	NZ/TMAZ interface on AS	
	403	7.9	83.4	43.9	NZ/TMAZ interface on RS	
Average	395	7.5	81.9	41.7		
B	383	5.0	79.4	27.8	NZ - AS	8.06
	387	6.0	80.2	33.3	NZ - AS	
	330	1.8	68.3	10.0	NZ/TMAZ interface on AS	
	337	3.2	69.9	17.8	NZ/TMAZ interface on AS	
	336	3.6	69.6	20.0	NZ – central area	
Average	355	3.9	73.5	21.8		
C	263	2.0	54.5	11.1	NZ/TMAZ interface on AS	6.46
	209	2.8	43.4	15.5	NZ/TMAZ interface on AS	
	164	1.5	33.9	8.3	NZ/TMAZ interface on AS	
	221	2.4	45.8	13.3	NZ/TMAZ interface on AS	
	327	3.6	67.7	20.0	NZ – central area	
	328	3.2	67.9	17.8	NZ – central area	
Average	252	2.6	52.2	14.3		
D	382	5.0	79.1	27.8	NZ/TMAZ interface on RS	5.00
	200	2.8	41.4	15.5	NZ/TMAZ interface on AS	
	409	6.5	84.8	36.1	NZ/TMAZ interface on AS	
	206	2.3	42.7	12.8	NZ/TMAZ interface on AS	
Average	299	4.2	62.0	23.0		
E	346	3.2	71.7	17.8	NZ/TMAZ interface on AS	10.21
	268	3.0	55.4	16.7	NZ/TMAZ interface on AS	
	337	2.8	69.8	15.5	NZ/TMAZ interface on AS	
Average	317	3.0	65.6	16.7		
G	391	5.6	81.0	31.1	NZ/TMAZ interface on RS	10.17
	403	6.9	83.4	38.3	NZ – RS	
	399	5.4	82.6	30.0	NZ/TMAZ interface on RS	
Average	398	6.0	82.3	33.1		
BM	481	18				

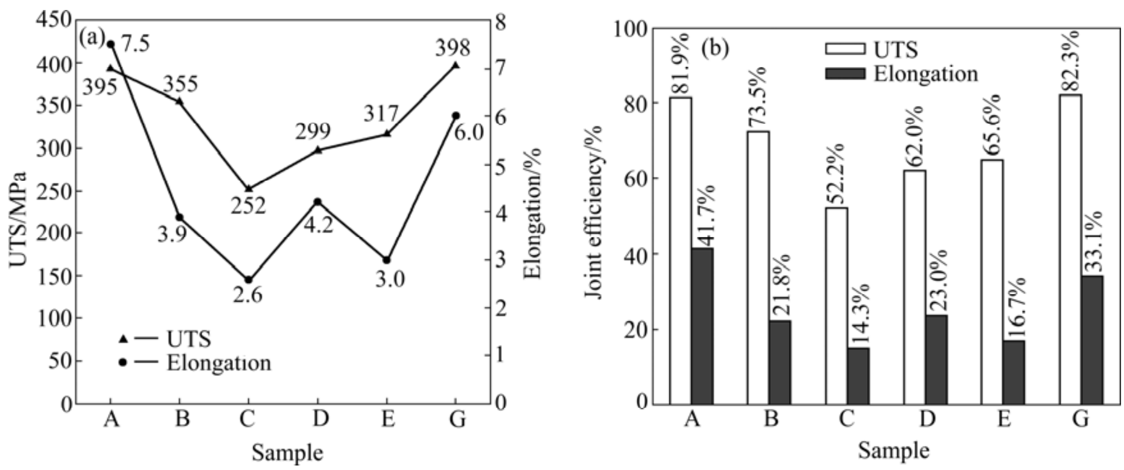

Fig. 13 Tensile properties and joint efficiency of joint

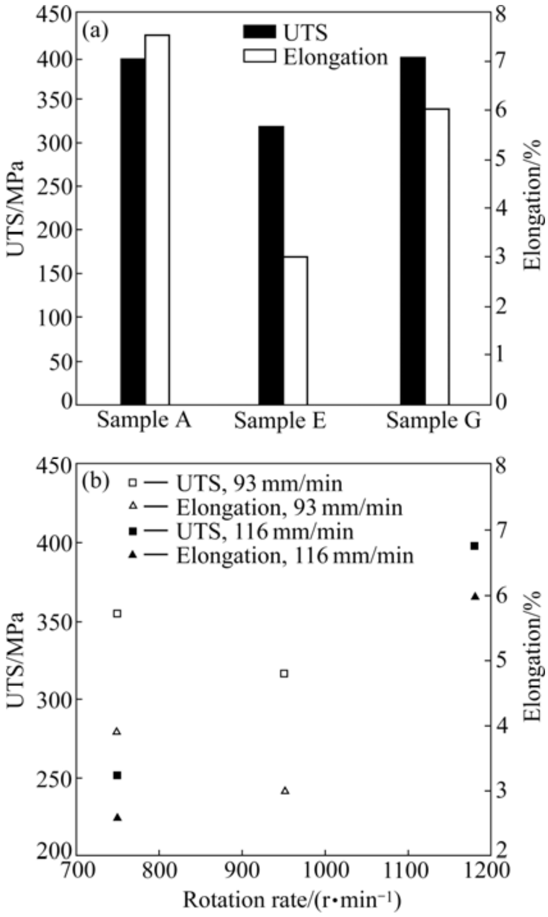

Fig. 14 Tensile properties of joints welded at approximately same R/v ratio (R/v≈10) (a), fixed welding speed and different rotation rate (b)

the joints was far lower than that of base material, and its maximum was 7.5%. The maximum UTS was obtained for sample G with ratio R/v=10.17. Samples A, E and G, welded with different parameters, but with similar R/v ratios (10.21, 10.27 and 10.17, respectively), showed different tensile properties (Fig. 14(a)). In terms of elongation the results were similar. If we consider UTS and elongation in terms of pseudo heat index R^2/v, it is clear that at similar ratio, the generated energy was not the same and was dependent on the used welding parameters, mainly rotation rate. For similar R/v or R^2/v ratio, increasing in ratio value was in good correlation with increasing in R or v, and they amounted approximately 20% per step. This implies that overall joint quality show strong dependence on combined effect of heat input and material flow states due to different welding parameters. In order to accurately determine tensile fracture location, the cross-sections of the specimen were etched, as shown in Fig. 15. In most case, fracture was located in contact line between NZ and TMAZ (Table 7).

4 Discussion

Welding power (Q) is calculated according to Eq. (1) suggested by HEURTIER et al [49] and experimentally verified by ABD EL-HAFEZ [50].

$$Q=\frac{2\pi}{3}\mu P\omega R_{\mathrm{s}}^{3} \tag{1}$$

where μ is the friction coefficient, P is the pressure (Pa), ω is the tool angular speed (rad/s), and R_s is the tool shoulder radius (m). HEURTIER et al [49] reported that the estimated average welding power, according to Eq. (1), for FSW of AA2024-T351 is 1.5 kW. Using conventional values of P=15 kN and μ=0.3 [50,51], the heat input (q) is calculated according to Eq. (2) [12].

$$q=\frac{2\pi}{3v}\mu F_{z}\omega R_{\mathrm{s}}\eta \tag{2}$$

where F_z is the axial force (kN), and v is the welding speed (mm/s). Since insufficient or excessive axial force can result in weld failure. This force plays a significant role in weld formation [52]. ARORA et al [26] reported that the axial force is significantly affected by shoulder diameter and slightly by the rotational and welding speed (Eq. (3)), whereas welding force is affected strongly by

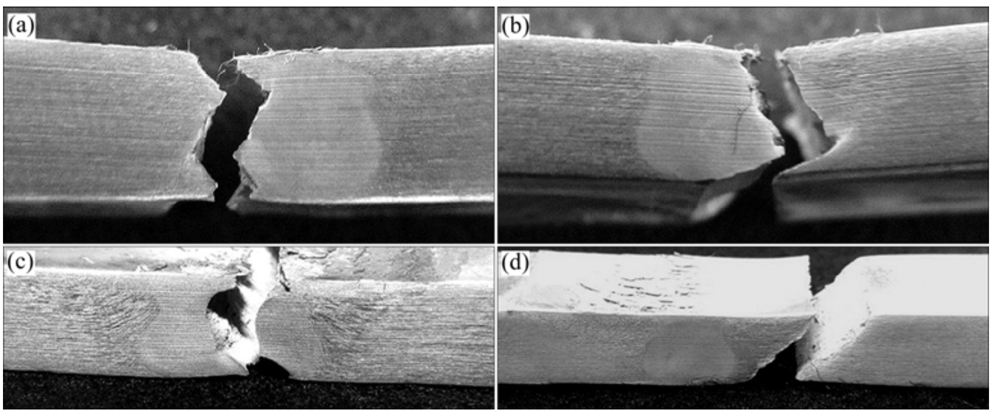

Fig. 15 Characteristic fracture location on tensile specimen: (a) NZ/TMAZ interface on AS; (b) NZ/TMAZ interface on RS; (c) NZ – central area; (d) TMAZ/HAZ interface on RS

Table 7 Summary of fracture location distribution

Fracture location	Number of fracture	Percent/%
NZ (central)	3	13
NZ (AS)	2	8
NZ (RS)	1	4
Total	6	25
NZ/TMAZ (AS)	13	54
NZ/TMAZ (RS)	4	17
Total	17	71
TMAZ/HAZ (AS)	0	0
TMAZ/HAZ (RS)	1	4
Total	1	4

welding speed and slightly by rotational speed and pin diameter (Eq. (4)). Furthermore, they suggested an empirical model for axial and welding force. The tensile strength of welds is significantly affected by welding speed and shoulder diameter whereas welding speed strongly affects the elongation [26].

$$F_z/\text{kN}=9.18R^{-0.312}v^{0.146}D^{2.78}d^{-0.121} \quad (3)$$

$$F_x/\text{kN}=478.2R^{-0.468}v^{0.646}D^{0.078}d^{0.523} \quad (4)$$

where R is the rotation rate (r/min), v is the welding speed (mm/min), D is the shoulder diameter (mm), and d is the pin diameter (mm).

The calculated values for weld power (Q), heat input (q), welding force (F_x) and axial force (F_z), according to Eq. (1) to (4) are shown in Table 8.

According to the equations it can be concluded that the rotation rate, welding speed, tool shoulder diameter and probe diameter are crucial parameters that affect FSW process forces, heat input and welding power. Increasing the welding speed causes two opposite effects: 1) increasing axial force; 2) decreasing heat input. Also, increasing rotation rate at the same welding speed leads to higher heat input and smaller F_x and F_z (Table 8). Welding power is increased significantly with the increase of rotation rate, while welding speed does not affect the power needed for FSW [46, 50, 53−55].

The obtained results suggested that weld appearance was more affected by rotation rate than by welding speed, due to differences in generated heat level (Fig. 3). Increasing R/v ratio leads to higher, both, heat input (expressed as pseudo-heat index R^2/v) and stirring increment, implying that the behavior is not uniform. Furthermore, it can be assumed that welding parameters and material flow have combined effect on weld appearance and they cannot be taken into consideration separately [25,29,32,43,54]. The obtained tunnel defects occurred in the case when material flow from retreating to advancing side around the pin was not adequate. As shown in Fig. 16, the tunnel mainly existed under the higher rotation rate and welding speed. When the welding speed was high, stirring effect of welding tool was waste. Probably this is the reason for tunnel defect occurrence. Similar opinions have been suggested by other authors [27,36,37,50,53].

Increasing R/v ratio leads to greater size of weld nugget—width and depth. This is due to a higher heat input and stirring increment owing to increased R/v ratio. Note that higher heat input improves material flow around tool pin. In other words, ‘‘revolutions per one millimeter’’ of the weld metal is increased by increasing R/v ratio. Therefore, a large amount of frictional heat and plastic-work are produced, and thus material easily flows and bigger NZ is formed [29,41,54]. Different spacing between rings is related to the pin forward movement per revolution, i.e., at a rotation rate of 750 and 1180 r/min and welding speed of 116 mm/min, the tool moves 0.1546 and 0.0983 mm/r, respectively [22,23,55].

The grain size revealed in the NZ and part of TMAZ is very fine. It is expected that, during very intensive deformation at high temperature, grain refinement is introduced by both deformation and recrystallization. There are also some opinions that even dynamic recrystallization can occur [15,56,57]. The fine and

Table 8 Calculated value for weld power, heat input, welding and axial force

Sample	Rotation rate, R/(r·min^{-1})	Welding speed, v/(mm·min^{-1})	Weld power, Q/kW	Heat input, q/(kJ·mm^{-1})	F_x/kN	F_z/kN	R/v	R^2/v
A	750	73	2.95	0.97	1.03	14.54	10.27	7700
B		93		0.76	1.20	15.06	8.06	6050
C		116		0.61	1.39	15.56	6.46	4850
D		150		0.47	1.64	16.15	5.00	3750
E	950	93	3.73	0.96	1.08	13.99	10.21	9700
F		190		0.47	1.71	15.53	5.00	4750
G	1180	116	4.63	0.96	1.12	13.51	10.17	12000
H		150		0.74	1.33	14.02	7.87	9280

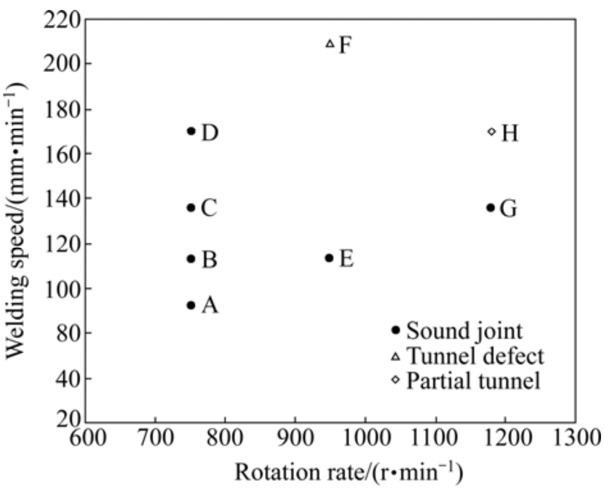

Fig. 16 Welding parameters versus FSW joint quality

equiaxed grains in NZ arise from exposure to severe plastic deformation and the greatest heat input during welding process. The elongated grains in TMAZ undergo less plastic deformation and lower heat input than NZ. On the other hand, in the HAZ plastic deformation is absent and only heat input plays a role, so the microstructure seems to be nonhomogenous, leading to increase in grain size. In TMAZ and HAZ, recrystallized phenomenon doesn't occur, but smaller precipitates may coarsen during welding process and notably the coarsened grains may be observed. Also, grain size is not the same in all parts of NZ. Grains are smaller at the bottom of the weld than at the center or top. It is assumed to be due to the differences in heat generated level, governing by distance from tool shoulder and backing plate. Therefore, hardness distributions show very strong dependence of the microstructure, and it is a direct indicator of microstructural evolution during FSW [18,24,26,30,32, 33,43,55,56,58].

The welds exhibited a W-shaped hardness profiles, typical for FSW joints of precipitate hardening aluminum alloy. The hardness profiles in general show that the FSW joints hardness is lower than that of the base metal. Hardness decreases in the HAZ and TMAZ, which are the softest zone in FSW joints. The NZ, TMAZ and HAZ are softer due to dissolution and coarsening of the strengthening precipitates during thermal cycle. It is assumed to be because of the heat generated during welding and subsequent recrystallization. Therefore, this effect is the greatest in TMAZ, while in the NZ is sluggish. Also, the ratio between the lowest hardness value in TMAZ and hardness of the base metal is close to the value of joint efficiency obtained from tensile properties [13,17,27,29,49]. Due to lack of symmetry, LHR hardness level and position (distance from weld center) depend on location across the weld as well as on welding parameters. In general, increasing the rotation rate at constant welding speed shows small to medium influence on LHR hardness and position, but increases the NZ hardness. On the other hand, as the welding speed increases, the hardness of softened zone also increases (Figs. 9 and 10) [27,40,44,50,54]. The detailed hardness distribution maps are in very good agreement with the normal strain distribution and yield stress map, reported by LOCKWOOD et al [16]. The tensile properties and fracture locations of the joints are in very good agreement and related to the hardness distributions.

Fracture of Al_2Cu particles is most intensive in the NZ, because this is the region through which tool pin passes, and thus experiences the highest deformation during stirring. On the other hand, it can be assumed that the presence of coarse Al_2Cu particles in TMAZ is the consequence of both stirring deformation and heat treatment [26]. It isn't clear that the presence of coarse Al_2Cu particles in TMAZ is only the consequence of material flow or both material flow and heat treatment.

The obtained values for UTS are in very good agreement with the expectation that FSW joints should have greater joint efficiency in comparison with the joints welded using traditional techniques. The welding parameters significantly affect the tensile properties of the FSW joints, but also they can be varied over a relatively wide range. The tensile properties of the joints are lower than those of the base material and the average value varies between 252 to 398 MPa. The maximum average tensile properties of 395 and 398 MPa and also joint efficiency of 81.9% and 82.3% were observed for R/v ratio of 10.27 and 10.17, respectively. Elongations are far lower than those of the base materials. The maximum elongation of 8.0% was obtained for ratio R/v=10.27, while the elongations of the other joints vary between 1.5% to 7.9%. The tensile properties results for R/v ratio of 10.21 are inferior probably due to non-adequate material condition during process, i.e. insufficient ratio between heat input and material flow [12,14,15,20,33,56, 59−61].

FSW joints mostly fractured along the LHR during tensile test. In most cases crack propagated along the contact line between NZ and TMAZ. It is assumed that this behavior can be related to the materials flow close to pin, i.e., probably the same feature that can introduce tunnel type defects [31,40,42,56]. FSW 2024-T351 joints would fracture at the NZ/TMAZ interface or at the NZ, even at TMAZ/HAZ interface, depending on the applied parameters. These findings remark that the influence of FSW parameters on void defects formation, mechanical properties and fracture behavior is complicated and not jet systematically investigated.

5 Conclusions

The influence of R/v ratio on joint quality in 2024-T351 aluminum alloy was established. The specimens were subjected to friction stir welding with the rotation rates of 750, 950 and 1180 r/min and welding speed between 73 and 190 mm/min, providing R/v ratio between 5.00 and 10.27. The welded joints were tested by means of both non-destructive (visual, penetrant and X-ray inspection) and destructive (metallographic, bending, tension and hardness) testing. Tensile efficiency of joints was in the range of 52.2% to 82.3%. Elongation efficiency was between 14.3% and 41.7%.

Microstructural features and mechanical properties could be effectively controlled by varying the rotation rate and welding speed.

The best quality of weld was obtained at R/v ratio of 8.06, 10.17 and 10.27. This behavior is attributed to the assumption that the material flows around the pin with optimal speed, i.e., sufficient amount of material is available to fill the gap and prevent tunnel formation.

Increasing of the R/v ratio leads to larger size of the NZ, and the formation of the finest onion rings structures.

The expected effect of attrition of Al_2Cu particle on mechanical properties is a higher fracture toughness and hardness in the weld zone.

The hardness distribution is in excellent agreement with the observed microstructures, showing two low hardness regions with almost equal values.

The tensile properties of the joints are lower than those of the base material, and the maximum efficiency in terms of UTS and elongation is 82.3% and 41.7%, respectively.

In most cases, crack propagated along the contact line between NZ and TMAZ, due to differences in microstructure of two zones.

Acknowledgments

The authors are indebted to Ministry of Education and Science of Serbia for financial support through Project TR34018. The authors also wish express their sincere thanks to Military Technical Institute of Serbian Army for technical support during performing friction stir welding experiments.

References

[1] LEFEBVRE F, GANGULY S, SINCLAIR I. Micromechanical aspects of fatigue in a MIG welded aluminum airframe alloy: Part 1. Microstructural characterization [J]. Materials Science and Engineering A, 2005, 397: 338−345.

[2] OWEN R A, PRESTON R V, WITHERS P J, SHERCLIFF H R, WEBSTER P J. Neutron and synchrotron measurements of residual strain in TIG welded aluminum alloy 2024 [J]. Materials Science and Engineering A, 2003, 346: 159−167.

[3] THOMAS W M, NICHOLAS E D, NEEDHAM J C, MURCH M G, TEMPLESMITH P, DAWES C J. GB Patent Application No. 9125978.8 [P]. 1991.

[4] PIRES J N, LOUREIRO A, BOLMSJO G. Welding robots [M]. Welding Technology, 2006: 27−71.

[5] VILAÇA P, THOMAS W. Friction stir welding technology [J]. Adv Struct Mater, 2012, 8: 85−124.

[6] MISHRA R S, MA Z Y. Friction stir welding and processing [J]. Materials Science and Engineering R, 2005, 50: 1−78.

[7] MISHRA R S, MAHONEY M W. Friction stir welding and processing [M]. Materials Park, Ohio, USA: ASM International, 2007.

[8] POSADA M, NGUYEN J P, FORREST D R, DELOACH J J. Friction stir welding advanced joining technology [J]. Amptiac Quarterly, 2003, 7: 13−20.

[9] GRUJICIC M, ARAKERE G, PANDURANGAN B, HARIHARAN A, YEN C F, CHEESEMAN B A. Development of a robust and cost-effective friction stir welding process for use in advanced military vehicles [J]. Journal of Materials Engineering and Performance, 2011, 20(1): 11−23.

[10] ERICSSON M, SANDSTROM R. Influence of welding speed on the fatigue of friction stir welds, and comparison with MIG and TIG [J]. International Journal of Fatigue, 2003, 25: 1379−1387.

[11] ELLIS M, STRANGWOOD M. Welding of rapidly solidified alloy 8009 (Al−8.5Fe−1.7Si−1.3V) — Preliminary study [J]. Materials Science and Technology, 1996, 12: 970−977.

[12] LAKSHMINARAYANAN A K, BALASUBRAMANIAN V, ELANGOVAN K. Effect of welding processes on tensile properties of AA6061 aluminum alloy joints [J]. International Journal of Advanced Manufacture Technology, 2009, 40: 286−296.

[13] SQUILLACE A, de FENZO A, GIORLEO G, BELLUCCI F. A comparison between FSW and TIG welding techniques: Modifications of microstructure and pitting corrosion resistance in AA 2024-T3 butt joints [J]. Journal of Materials Processing and Technology, 2004, 152: 97−105.

[14] HE Zhen-bo, PENG Yong-yi, YIN Zhi-min, LEI Xue-feng. Comparison of FSW and TIG welded joints in Al−Mg−Mn−Sc−Zr alloy plates [J]. Transactions of Nonferrous Metals Society of China, 2011, 21: 1685−1691.

[15] MALARVIZHI S, BALASUBRAMANIAN V. Effect of welding processes on AA2219 aluminum alloy joint properties [J]. Transactions of Nonferrous Metals Society of China, 2011, 21: 962−973.

[16] LOCKWOOD W D, TOMAZ B, REYNOLDS A P. Mechanical response of friction stir welded AA 2024: Experiment and modelling [J]. Materials Science and Engineering A, 2002, 323: 348−353.

[17] ALI A, BROWN M W, RODOPOULOS C A, GARDINER S. Characterization of 2024-T351 friction stir welding joints [J]. Journal of Failure Analysis and Prevention, 2006, 6: 83−96.

[18] BOOTH D P, STARINK M J, SINCLAIR I. Analysis of local microstructure and hardness of 13 mm gauge 2024-T351 AA friction stir welds [J]. Materials Science and Technology, 2007, 23: 276−284.

[19] GOLESTANEH A F, ALI A, ZADEH M. Modeling the fatigue crack growth in friction stir welded joint of 2024-T351 Al alloy [J],

Materials and Design, 2009, 30: 2928−2937.

[20] DI S S, YANG X Q, LUAN G H, JIANG B. Comparative study on fatigue properties between AA2024-T4 friction stir welds and base materials [J]. Materials Science and Engineering A, 2006, 435−436: 389−395.

[21] ALI A, AN X, RODOPOULOS C A, BROWN M W, O'HARA P, LEVERS A, GARDINER S. The effect of controlled shot peening on the fatigue behavior of 2024-T3 aluminum friction stir welds [J]. International Journal of Fatigue, 2007, 29: 1531−1545.

[22] KRISHNAN K N. On the formation of onion rings in friction stir welds [J]. Materials Science and Engineering A, 2002, 327: 246−251.

[23] SUTTON M A, YANG B, REYNOLDS A P, TAYLOR R, Microstructural studies of friction stir welds in 2024-T3 aluminum [J]. Materials Science and Engineering A, 2002, 323: 160−166.

[24] YANG B, YAN J, SUTTON M, REYNOLDS A. Banded microstructure in AA2024-T351 and AA2524-T351 aluminum friction stir weld: Part I. Metallurgical studies [J]. Materials Science and Engineering A, 2004, 364: 55−65.

[25] SCHMIDT H, DICKERSON T, HATTEL J. Material flow in butt friction stir welds in AA2024-T3 [J]. Acta Materialia, 2006, 54: 1199−1209.

[26] ARORA K, PANDEY S, SCHAPER M, KUMAR R. Effect of process parameters on friction stir welding of aluminum alloy 2219-T87 [J]. International Journal of Advanced Manufacture Technology, 2010, 50: 941−952.

[27] ZHANG Z, XIAO B L, MA Z Y. Effect of welding parameters on microstructure and mechanical properties of friction stir welded 2219Al-T6 joints [J]. Journal of Materials Science, 2012, DOI: 10.1007/s10853-012-6261-1.

[28] BIALLAS G, BRAUN R, DALLE DONNE C D, STANIEK G, KAYSSER W. Mechanical properties and corrosion behavior of friction stir welded 2024-T3 [C]// Proceedings of the 1st International Symposium on Friction Stir Welding. Thousand Oaks, CA, 1999: 14−16.

[29] HASSAN K, PRANGNELL P, NORMAN A, PRICE D, WILLIAMS S. Effect of welding parameters on nugget zone microstructure and properties in high strength aluminium alloy friction stir welds [J]. Science and Technology of Welding and Joining, 2003, 8: 257−268.

[30] HASSAN K, NORMAN A, PRICE D, PRANGNELL P. Stability of nugget zone grain structures in high strength Al alloy friction stir welds during solution treatment [J]. Acta Materialia, 2003, 51: 1923−1936.

[31] LIU H, FUJII H, MAEDA M, NOGI K. Tensile properties and fracture locations of friction-stir-welded joints of 2017-T351 aluminum alloy [J]. Journal of Materials Processing Technology, 2003, 142: 692−696.

[32] XU Wei-feng, LIU Jin-he, LUAN Guo-hong, DONG Chun-lin. Temperature evolution, microstructure and mechanical properties of friction stir welded thick 2219-O aluminum alloy joints [J]. Materials and Design, 2009, 30: 1886−1893.

[33] LIU Hui-jie, ZHANG Hui-jie, PAN Qing, YU Lei. Effect of friction stir welding parameters on microstructural characteristics and mechanical properties of 2219-T6 aluminum alloy joints [J]. International Journal Materials Forming, 2011, DOI: 10.1007/s12289-011-1048-5.

[34] KUMAR K, KAILAS S. The role of friction stir welding tool on material flow and weld formation [J]. Materials Science and Engineering A, 2008, 485: 367−374.

[35] ARBEGAST W. A flow-partitioned deformation zone model for defect formation during friction stir welding [J]. Scripta Materialia, 2008, 58: 372−376.

[36] ZHANG Z, XIAO B L, WANG D, MA Z Y. Effect of alclad layer on material flow and defect formation in friction stir welded 2024 aluminum alloy [J]. Metallurgical and Materials Transactions A, 2011, 42: 1717−1726.

[37] GHARACHEH A, KOKABI A H, DANESHI G H, SHALCHI B, SARRAFI R. The influence of the ratio of "rotational speed/traverse speed" (o/v) on mechanical properties of AZ31 friction stir welds [J]. International Journal of Machine Tools & Manufacture, 2006, 46: 1983−1987.

[38] RADISAVLJEVIC I, RADOVIC N, GRABULOV V, ZIVKOVIC A. Influence of process parameters on tunnel type defect appearance and weld quality in FSW welded Al 2024 plates [C]// 5th International Scientific Conference on Defensive Technologies OTEH 2012. Belgrade: Military Technical Institute, 2012: 625−630.

[39] REN S R, MA Z Y, CHEN L Q. Effect of welding parameters on tensile properties and fracture behavior of friction stir welded Al–Mg–Si alloy [J]. Scripta Materialia, 2007, 56: 69−72.

[40] LIU F C, MA Z Y. Influence of tool dimension and welding parameters on microstructure and mechanical properties of friction stir welded 6061-T651 aluminum alloy [J]. Metallurgical and Materials Transaction A, 2008, 39: 2378−2388.

[41] LIM S, KIM S, LEE C, KIM S. Tensile behavior of friction-stir-welded Al 6061-T651 [J]. Metallurgical and Materials Transaction A, 2004, 35: 2829−2835.

[42] GENEVOIS C, DESCHAMPS A, VACHER P. Comparative study on local and global mechanical properties of 2024-T351, 2024-T6 and 5251-O friction stir welds [J]. Materials and Science Engineering A, 2006, 415: 162−170.

[43] ELANGOVAN K, BALASUBRAMANIAN V. Influences of tool pin profile and welding speed on the formation of friction stir processing zone in AA2219 aluminium alloy [J]. Journal of Materials Processing Technology, 2008, 200: 163−175.

[44] LAKSHMINARAYANAN A K, MALARVIZHI S, BALASUBRAMANIAN V. Developing friction stir welding window for AA2219 aluminum alloy [J]. Transactions of Nonferrous Metals Society of China, 2011, 21: 2339−2347.

[45] RAZAL ROSE A, MANISEKAR K, BALASUBRAMANIAN V. Effect of axial force on microstructure and tensile properties of friction stir welded AZ61A magnesium alloy [J]. Transactions of Nonferrous Metals Society of China, 2011, 21: 974−984.

[46] KUMAR R, SINGH K, PANDEY S. Process forces and heat input as function of process parameters in AA5083 friction stir welds [J]. Transactions of Nonferrous Metals Society of China, 2012, 22: 288−298.

[47] VILACA P, QUINTINO L, DOS SANTOS J F. iSTIR—Analytical thermal model for friction stir welding [J]. Journal of Materials Processing Technology, 2005, 169: 452−465.

[48] ARBEGAST W J, HARTLEY P J. Friction stir weld technology development at Lockheed Martin Michoud space system—An overview [C]// 5th International Conference of Trends in Welding Research. Pine Mountain, GA, 1998: 541.

[49] HEURTIER P, JONES M J, DESRAYAUD C, DRIVER J H, MONTHEILLET F, ALLEHAUX D. Mechanical and thermal modeling of friction stir welding [J]. Journal of Materials Processing Technology, 2006, 171: 348−357.

[50] ABD EL-HAFEZ H. Mechanical properties and welding power of friction stirred AA2024-T35 joints [J]. Journal of Materials

Engineering Performance, 2011, 20: 839−845.

[51] SCHMIDT H, HATTEL J, WERT J. An analytical model for the heat generation in friction stir welding [J]. Modeling and Simulation in Materials Science and Engineering, 2004, 12: 143−157.

[52] KUMAR K, KAILAS S. On the role of axial load and the effect of interface position on the tensile strength of a friction stir welded aluminum alloy [J]. Materials and Design, 2008, 29: 791−797.

[53] ZHANG Z, ZHANG H W. Numerical studies on the effect of transverse speed in friction stir welding [J]. Materials and Design, 2009, 30: 900−907.

[54] ZHANG X X, XIAO B L, MA Z Y. A transient thermal model for friction stir weld: Part II. Effects of weld conditions [J]. Metallurgical and Materials Transaction A, 2011, 42: 3229−3239.

[55] ZHANG Z, ZHANG H W. A fully coupled thermo-mechanical model of friction stir welding [J]. International Journal of Advanced Manufacturing Technology, 2008, 37: 279−293.

[56] SRIVATSAN T, VASUDEVAN S, PARK L. The tensile deformation and fracture behavior of friction stir welded aluminum alloy 2024 [J]. Materials Science and Engineering A, 2007, 466: 235−245.

[57] JATA K V, SEMIATIN S L. Continuous dynamic recrystallization during friction stir welding of high strength aluminum alloys [J]. Scripta Materialia, 2000, 43: 743−749.

[58] JONES M J, HEURTIER P, DESRAYAUD C, MONTHEILLET F, ALLEHAUX D, DRIVER J H. Correlation between microstructure and microhardness in a friction stir welded 2024 aluminum alloy [J]. Scripta Materialia, 2005, 52: 693−697.

[59] LIU H J, FUJII H, NOGI K. Friction stir welding characteristics of 2017-T351 aluminum alloy sheet [J]. Journal of Materials Science, 2005, 40: 3297−3299.

[60] STROMBECK A, SANTOS J, TORSTER F, LAUREANO P, KOCAK M. Fracture toughness behavior of FSW joints on aluminum alloys [C]// 1st International Symposium on Friction Stir Welding. Thousand Oaks, CA, 1999. Paper No. S9-P1.

[61] AYDIN H, BAYRAM A, UGUZ A, AKAY K S. Tensile properties of friction stir welded joints of 2024 aluminum alloys in different heat-treated-state [J]. Materials and Design, 2009, 30: 2211−2221.

搅拌摩擦焊工艺参数对 2024-T351 铝合金搭接焊接头成形质量和力学性能的影响

I. RADISAVLJEVIC[1], A. ZIVKOVIC[2], N. RADOVIC[3], V. GRABULOV[4]

1. Military Technical Institute, Belgrade, Serbia;
2. GOSA FOM, Smederevska Palanka, Serbia;
3. Faculty of Technology and Metallurgy, University of Belgrade, Belgrade, Serbia;
4. Institute for Materials testing, Belgrade, Serbia

摘　要：研究搅拌摩擦焊时 R/v 比对 2024-T351 铝合金焊接质量的影响。搅拌摩擦焊时搅拌针的旋转速度设定为 750、950 和 1180 r/min，焊接速度在 73~190 mm/min 内变化，对应的 R/v 比在 5.00~10.27 内。采用各种无损(外观检测、X 射线检测)和有损(金相观察、拉伸实验和硬度测量)检测手段对焊接试样进行分析。在所有的试样中，搅拌摩擦焊中各种典型的区域都有存在，不同的区域其晶粒尺寸不同。接头的拉伸性能为基材的 52.2%~82.3%。在 R/v 比为 8.06，10.17 和 10.27 时焊接质量最佳。其原因是在最佳搅拌速度下，材料围绕搅拌针充分流动，从而能够填充其中产生的空隙，阻止空洞的生成。结果还表明，R/v 比对接头的硬度分布、洋葱样形状、裂纹的萌生和扩展都有影响。

关键词：2024 铝合金；搅拌摩擦焊；焊接参数；热量输入；焊接质量

(Edited by Sai-qian YUAN)